Hybrid-ARQ-Aided Short Fountain Codes Designed for Block-Fading Channels

Hong Chen, Robert G. Maunder, *Member, IEEE*, Yi Ma, *Senior Member, IEEE*, Rahim Tafazolli, *Senior Member, IEEE*, and Lajos Hanzo, *Fellow, IEEE*

***Abstract*—As a benefit of their inherent rateless nature, fountain codes constitute a favorable choice for protecting packet-based transmissions in the physical layer for wireless channels having varying quality. However, previous research has revealed that the performance of fountain codes substantially degrades as their block length is reduced. Three structural phenomena of the Tanner graph were identified by Mackay in the hard decoding of fountain codes on binary erasure channels (BECs), which may be referred to as having "no degree-one check nodes (CNs)," "no emerging degree-one CNs," and "uncovered variable nodes (VNs)." In this paper, we explicitly analyzed how these structural phenomena influence their soft decoding algorithm. Furthermore, these phenomena are shown to be responsible for the high error floors when fountain codes are transmitted over noisy fading channels, particularly for the transmissions of short blocks. To eliminate the influence of these structural phenomena, we conceived a technique of generating a few specifically encoded bits with the aid of the associated Tanner graph. Simulation results have demonstrated that our improved Raptor (IRaptor) codes significantly reduce the packet loss ratio (PLR) of conventional fountain codes, despite imposing reduced low complexity. Finally, we conceive a novel adaptive hybrid automatic repeat request (HARQ) scheme based on a lookup table (LUT)-aided technique, which may adapt its coding rate for each transmission. Our simulation results demonstrated that the proposed IRaptor HARQ achieves a similar performance to the Long-Term Evolution (LTE) turbo-coded HARQ scheme or even outperforms the LTE arrangement for block length in excess of 1000 bits.**

***Index Terms*—Author, please supply index terms/keywords for your paper. To download the IEEE Taxonomy go to http://www.ieee.org/documents/taxonomy_v101.pdf.**

AQ1

I. Introduction

In recent years, fountain codes [1]–[3] have attracted substantial attention since they are capable of approaching the capacity of binary erasure channels (BECs). Hence, most publications focus on protecting the transmission of packets over BECs. Additionally, their rateless property facilitates code-rate adaptation based on the near-instantaneous channel quality.

The rateless property is capable of achieving the highest possible throughput, while approaching a potentially zero outage probability. Therefore, Erez *et al.,* [4] studied the construction of rateless codes based on traditional fixed-rate codes originally conceived for Gaussian channels. To obtain the rateless property, Chen *et al.,* [5] proposed a Raptor-like method, which may extend a low-density parity-check (LDPC) precode from an initial coding rate to any arbitrary rates. Due to the inherent rateless feature of fountain codes, in [6]–[12], the performance of fountain codes employed as a channel code in the physical layer for transmission over noisy fading channels was studied. More specifically, Palanki and Yedidia [6] revealed that Luby transform (LT) codes suffer from error floors, whereas Raptor codes [7] may achieve a lower bit error ratio (BER) than that of LT codes. However, Kasai and Sakaniwa [12] indicated that Raptor codes also exhibit high error floors and designed their outer code as a multiplicative repetition code, while adopting a nonbinary LDPC inner code for improving the performance. Etesami and Shokrollahi [8] derived the necessary conditions of arriving at an optimal degree distribution for transmission over binary memoryless symmetric channels. Furthermore, Cheng *et al.,* [11] demonstrated that Raptor codes may fail to achieve capacity, when the channel's SNR lies outside a specific SNR interval.

However, the performance of fountain codes over noisy channels is not as appealing as anticipated by the given studies under idealized simplifying assumptions, not even at high block lengths. For example, LT codes and Raptor codes have high error floors, as shown in [6] and [12], whereas in [7], the discrepancy between the average rate of Raptor codes and the channel capacity was quantified. Moreover, the performance degrades dramatically, when fountain codes are invoked for protecting short blocks. As our new contribution, we reveal that the modest performance of fountain codes is not only due to having undesirable channel conditions but owing to having a suboptimum Tanner graph structure as well. Tanner graphs [13] efficiently visualize the encoding and decoding process of fountain codes. We analyze how a set of three structural phenomena of the Tanner graph as identified by Mackay in the hard decoding of fountain codes [1] degrades their soft decision. These phenomena are: having "no degree-one check nodes (CNs)," "no emerging degree-one CNs," and the presence of "uncovered variable nodes (VNs)," which again degrade the achievable performance of their soft decoding.

Manuscript received January 24, 2013; revised October 18, 2014 and December 20, 2014; accepted January 2, 2015. The work of L. Hanzo was supported by the European Research Council under its Advanced Fellow Grant. The work of H. Chen was supported by the National Natural Science Foundation of China under Grant 61401067. The review of this paper was coordinated by C. Ibars.

H. Chen, Y. Ma, and R. Tafazolli are with the University of Electronic Science and Technology, Chengdu 610051, China, and also with the Centre for Communication Systems Research (CCSR), University of Surrey, GU2 7XH Surrey, U.K.

R. G. Maunder and L. Hanzo are with the School of Electronics and Computer Science, University of Southampton, SO17 1BJ Southampton, U.K.

Digital Object Identifier 10.1109/TVT.2015.2388632

We show that the occurrence of these phenomena is mitigated although not entirely eliminated—by the family of systematic fountain codes [14] and by the degree distributions relying on high-degree fractions [1], [3]. Following this, when aiming for transmitting short blocks, we conceive improved Raptor (IRaptor) codes by employing our new technique of transmitting several specifically encoded bits, which are carefully generated for eliminating these three structural phenomena of the Tanner graph. A simple degree distribution may be adopted with the aid of these specifically encoded bits. As a result, the SNR required at a given packet loss ratio (PLR) reduced by more than 1.5 dB, despite the fact that the decoding complexity is halved compared with that of conventional systematic fountain codes.

Furthermore, we combine IRaptor codes with hybrid automatic repeat request (HARQ) in order to construct an adaptive HARQ scheme. In our proposed IRaptor-coded HARQ scheme, the transmitter is informed about the channel quality by the channel quality indicator (CQI) messages fed back from the receiver. As a benefit, it becomes capable of chasing the appropriate coding rate, regardless of the specific channel conditions. It is also capable of passing/delaying its transmissions, if the channel is deemed to be in deep fade.

In [12], the "high-error-floor problem" of conventional fountains codes, which was achieved by using a repetition code as their inner code and adopting a nonbinary LDPC outer code, has been carefully addressed. Both the multiplicative repetition code and the nonbinary LDPC code rely on operations over GF(2^m)($m > 1$), instead of the simpler exclusive-OR (XOR)-based addition of bits as in conventional Raptor codes. Compared with our IRaptor codes, it transpires that this implies having a significantly higher encoding and decoding complexity. Moreover, the multiplicative repetition inner code introduced in [12] actually operates as an LT-like code in conjunction with a specific degree distribution, which cannot guarantee circumventing any of the aforementioned three structural phenomena of the corresponding Tanner graph. Based on the analysis of Section II-B, we infer that these structural phenomena may inject decoding errors into the outer LDPC code, which may exceed its correction capability. Therefore, we may reasonably hypothesize that our IRaptor codes compare well with the multiplicatively repeated nonbinary LDPC codes proposed in [12]. These issues may be explored in our future work.

Chen *et al.*, [5] attempted to propagate the rateless property to the class of LDPC codes. To reduce the coding rate, they used LT-like encoding methods for generating more VNs based on a LDPC precoder having an initial coding rate. More specifically, a conventional LDPC precoder first generates an appropriate number of VNs for the sake of arriving at an initial coding rate based on an optimized protograph. This protograph is then optimally extended each time, when a new VN and a new CN are added into it, until a final coding rate is reached. When comparing it to our IRaptor codes, this Raptor-like LDPC code has a more complex encoding process since finding the optimal protograph will be repeated many times while arriving from the initial coding rate to the required coding rate. Furthermore, the final extended protograph represents the LDPC code's parity-check matrix, which has to be transformed to the generator matrix for encoding, hence, further increasing the encoding complexity as well. We may present a quantitative performance comparison between the family of Raptor-like LDPC codes and our IRaptor codes in our future research.

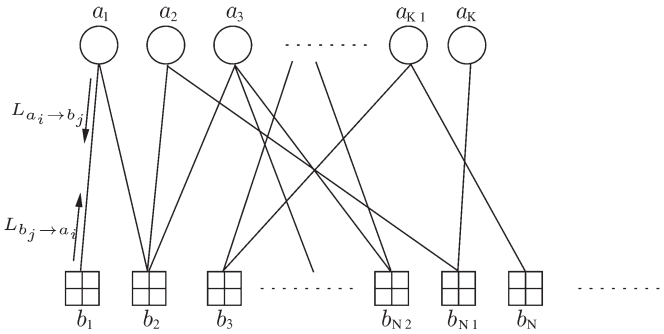

Fig. 1. Tanner graph representing fountain codes, where the hollow circles denote source bits. Each square represents an encoded bit generated by the bitwise XOR sum of its connected source bits.

The organization of this paper is as follows. In Section II, we briefly introduce soft fountain codes and analyze the corresponding Tanner graph. A novel method is proposed in Section III for improving the performance for the transmissions of finite-length blocks. Our simulation results are presented in Section III-B for characterizing our IRaptor codes in contrast to both conventional fountain codes and to the Long-Term Evolution (LTE) system's turbo codes [15]. Additionally, the IRaptor codes will be combined with HARQ in Section IV, where the turbo-coded HARQ of the LTE standard is chosen as the most powerful existing benchmarker. Finally, Section V offers our conclusions.

II. Fountain Codes

Fountain codes are known for its capability of producing an endless supply of encoded symbols for a block of source symbols, each having a length of 1 bit in this paper. They may be visually characterized by a Tanner graph, as shown in Fig. 1, where circles denote the so-called VNs and squares denote CNs.

More explicitly, the fountain encoder outputs a sequence of encoded bits $b_1, b_2, \ldots, b_N$ for a block of source bits $a_1, a_2, \ldots, a_K$. Each encoded bit b_j is generated by modulo-2 adding several randomly chosen source bits a_{d_i}, where $d_i \in \Omega_j$ and Ω_j is the set formed by all the connections by which the source bits a_{d_i} are connected with the encoded bit b_j, as shown in Fig. 1. Mathematically, each encoded bit is generated by

$$b_j = a_{d_1} \oplus a_{d_2} \cdots \oplus a_{d_v}, \qquad (d_1, d_2, \ldots, d_v \in \Omega_j). \quad (1)$$

The number of source bits v in the set Ω_j is referred to as the "degree" of that encoded bit, which is a random variable following a specific degree distribution. Furthermore, the positions (represented by d_i) of these source bits involved in generating each encoded bit are evenly distributed in the block region $[1, K]$.

A. Soft Decoding

LT codes [2] constitute a family of practical fountain codes, which rely on the belief propagation algorithm for simplifying the hard decoding of encoded packets received over BECs. When they act as channel codes in the physical layer, their soft decoding relying on the sum product algorithm [16] based on belief propagation is also feasible for transmissions over noisy fading channels [17]–[19]. Note that only N_t successfully received packets are involved in the hard decoding of LT codes received over BECs, whereas the other $(N - N_t)$ encoded packets have been erased owing to their corruption or due to network congestion.

However, all N encoded bits will assist the soft decoding of LT codes over noisy fading channels. Explicitly, the receiver is capable of reconstructing the same Tanner graph as the transmitter with the aid of a pseudorandom generator or by using some side information passed along with the transmitted bits. Then, soft information will be iteratively exchanged along the edges between the CNs and VNs of this Tanner graph, as shown in Fig. 1, where $L^{(m)}_{b_j \to a_i}$ represents the log likelihood ratios (LLRs) passed from the CNs b_j to the VNs a_i at the mth iteration, whereas $L^{(m)}_{a_i \to b_j}$ represents the LLRs passed from the VNs a_i to the CNs b_j at the mth iteration. The following two equations are calculated in turn during the iterative decoding [16], [20]:

$$L^{(m)}_{b_j \to a_i} = \tilde{b}_j \boxplus \left(\sum_{i' \in \Omega_j, i' \neq i} \boxplus \left(L^{(m-1)}_{a_{i'} \to b_j} \right) \right) \tag{2}$$

$$L^{(m)}_{a_i \to b_j} = \sum_{j' \in \Psi_i, j' \neq j} L^{(m)}_{b_{j'} \to a_i} \tag{3}$$

where $\tilde{b}_j$ represents the channel's output LLR corresponding to the encoded bit b_j and the set Ψ_i is formed of all CNs connected to the single VN a_i in a way similar to the set of connections Ω_j defined before. Furthermore, $\boxplus$ is referred to as the box-plus operation, where the box-plus of two LLR values may be specifically expressed as [21]

$$L_1 \boxplus L_2 = \text{sign}(L_1) \cdot \text{sign}(L_2) \cdot \min\{|L_1|, |L_2|\} + f(\cdot) \tag{4}$$

with $f(\cdot)$ being a correction term, which may be stored in a lookup table (LUT), based on quantized versions of the accurate expression of $\log(1 + e^{(-|L_1+L_2|)}) - \log(1 + e^{(-|L_1-L_2|)})$. Furthermore, the box-plus operator defined for two LLRs in (4) can be extended to more LLRs by exploiting the associativity of the box-plus operator.

Iterative decoding starts from (2), calculating the extrinsic LLRs $L^{(m)}_{b_j \to a_i}$ for each edge and for all CNs in Fig. 1. In the first computation of (2), the initial *a priori* LLRs of $L^{(0)}_{a_i \to b_j}$ are set to zeros. The outputs $L^{(1)}_{b_j \to a_i}$ will be used as the *a priori* LLRs in (3). The next evaluation of (3) calculates the corresponding extrinsic LLRs $L^{(1)}_{a_i \to b_j}$ for all VNs. This may provide increased *a priori* LLRs $L^{(1)}_{a_i \to b_j}$ fed back to (2) for the second round of calculations. After invoking (2) in each iteration, a hard decision may be made on the *a posteriori* LLRs of $\tilde{\mathbf{a}}$, where each element may be calculated as

$$\tilde{a}_i = \sum_{j \in \Psi_i} L_{b_j \to a_i}. \tag{5}$$

Then, the iterations continue until a successful recovery detected by a CRC or convergence is achieved when no extrinsic information can be obtained.

B. Tanner Graph Analysis

MacKay explained in [1] that the degree-one CNs play a critical role in the hard decoding of LT codes. He demonstrated that a desired degree distribution should produce many low-degree CNs to facilitate the commencement of the decoding process and to keep it going while additionally generating a small fraction of high-degree CNs to protect all source packets. However, the actual degree distribution may deviate from the originally designed distribution, unless the block length is sufficiently long. For short block lengths, this deviation also leads to a deficient Tanner graph exhibiting an unfavorable structure, as identified by Mackay [1], namely, having "no degree-one CNs," "no emerging degree-one CNs" and "uncovered VNs." At first glance, the LT soft decoding described in Section II-A remains unaffected by the Tanner graph's structure. However, here, we will analyze these structural phenomena of the Tanner graph, which significantly degrade the attainable soft decoding performance of fountain codes for transmission over noisy fading channels, albeit they have neither been mentioned in [6]–[11] nor been explicitly exploited by MacKay.

1) No Degree-One CNs: By examining (4), we can infer that its result can only be a valid nonzero value, when both $L1$ and $L2$ are nonzero. Therefore, initially only the channel LLRs $\tilde{b}_j$ connected to a degree-one CN may be passed to the edges of the Tanner graph by observing (2), since all initial LLRs $L^{(0)}_{a_i \to b_j}$ have a value of zero. Then, the iterative LT soft decoding process has to be triggered by at least one degree-one CN.

2) No Emerging "Degree-One" CNs: The success of seamlessly continued iterations depends on encountering at least one new "degree-one" CN emerging at each iteration. This "degree-one" CN is not a real degree-one CN connected to a single VN as stated in [1]. Instead, there are some CNs in the Tanner graph that have a degree higher than one in the presence of zero *a priori* LLRs, i.e., no *a priori* information. However, when all *a priori* LLRs along all other edges that are involved for calculating the extrinsic LLR of one of the edges of this CN become nonzero, these corresponding input edges of this CN may be deemed to be removed. Hypothetically speaking, we may be left with a single edge awaiting the calculation of its extrinsic LLR at this particular CN. Hence, we might refer to these in quotation mark, as "hypothetical degree-one" CNs in the soft decoding.

For example, assume that the encoded bit b_1 has an original degree of two, connecting the source bit a_1 and a_2. On evaluating $L^{(2)}_{b_1 \to a_1} = \tilde{b}_1 \boxplus L^{(1)}_{a_2 \to b_1}$ in the second iteration, $L^{(1)}_{a_2 \to b_1}$ will act as the *a priori* LLR, provided that it becomes a nonzero value after evaluating (3) in the first iteration. Since all

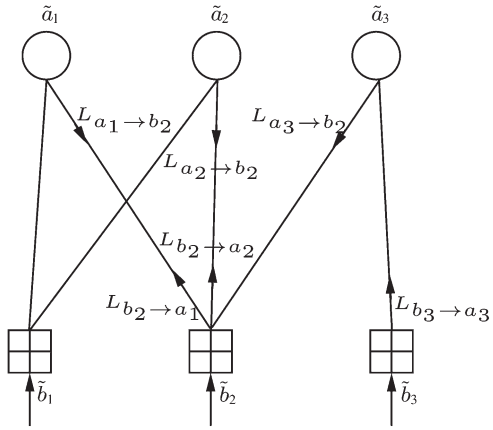

Fig. 2. Tanner graph where no new "degree-none" CN will emerge at the second iteration.

operands are nonzero here, an increased nonzero $L^{(2)}_{b_1 \to a_1}$ may be obtained. In this way, the channel LLR $\tilde{b}_1$ may be invoked within the Tanner graph for assisting the rest of the iterative decoding process.

Nonetheless, there exists a specific Tanner graph structure, where no new "hypothetical degree-one" CNs appear at some stage; hence, the remainder of the CNs are left without a "hypothetical degree-one" node, and as a result, the corresponding channel LLRs become "helpless." Fig. 2 shows an example of this structure, where the decoding performance fails to improve after the first iteration. No new nonzero LLRs may be obtained during the second iteration or in fact not even during the ensuing later iterations. In this example, The channel LLRs $\tilde{b}_1$ and $\tilde{b}_2$ are never entered into the graph; hence, they become unexploited, i.e., useless.

3) Uncovered VNs: As aforementioned, a small fraction of high-degree CNs is likely to avoid the absence of some source bits among the encoded bits, albeit this increases the fountain codes' decoding complexity. Hence, Raptor codes [3] invoke LDPC codes as their outer code for decoding the uncovered source bits, so that the inner LT code may adopt a component degree distribution imposing reduced complexity.

Despite the lower complexity of the inner LT codes, Raptor codes' recent studies [3], [8], [9] ignore the LDPC decoding complexity, although in this light their complexity contribution is substantial. Moreover, the degree distribution of the inner LT codes in [3] also contains several terms having a high degree, e.g., the degree terms of 64 and 65. Therefore, the overall complexity of Raptor codes may become unattractive.

III. Improved Fountain Codes

Systematic fountain codes [14] automatically and naturally solve the problems of having "no degree-one CNs" and "uncovered VNs" in the Tanner graph by transmitting all the original information bits before the fountain encoded parity bits. However, the problem of having "no emerging degree-one CNs"—as mentioned in Section II-B—still exists in systematic fountain codes.

TABLE I
Recorded Lists for the Tanner Graph of Fig. 2

CN index	Lists
1	{1,2}
2	{1,2,3}
3	{3}
VN index	**Lists**
1	{1,2}
2	{1,2}
3	{2,3}

For nonsystematic fountain codes, regardless of how good the channel conditions are, the attainable performance may be degraded by the above three potential features of the Tanner graph. Based on the fact that the encoder and decoder rely on the same Tanner graph, these structural phenomena may be eliminated by the encoder since it is potentially capable of adjusting the Tanner graph structure after generating a specific number of encoded bits.

A. Solutions for Improving the Tanner Graph

To realize this Tanner graph construction, we allocate a list for each VN and each CN to record the indexes of its connected counterparts. As for the lists of CNs, they are simply formed once an encoded bit is created, whereas the lists of VNs are dynamically filled during the generation of each encoded bit. For example, when considering the Tanner graph of Fig. 2, the list of CN 1 is {1, 2}, storing the indexes of its connected VNs when CN 1 is generated. Simultaneously, this CN's list component at index 1 is in turn appended to the lists of those VNs that it is connected to, namely to VN 1 and VN 2 in our specific example. Finally, once three encoded bits have been generated, all recorded lists are as shown in Table I.

With the aid of these lists, we are now ready to solve the potential problems caused by the Tanner graph's structure. After a number of encoded bits have been generated, the encoder may readily spot the occurrence of "no degree-one CNs" and "uncovered VNs" by inspecting the recorded lists of CNs and VNs. To eliminate the occurrence of "no degree-one CNs," the encoder will generate a new degree-one CN in the usual way. For eliminating "uncovered VNs," the encoder produces the corresponding number of CNs with a random degree plus one, where the random degree indicates the VNs randomly selected with an identical probability, whereas the additional one corresponds to the one among the uncovered VNs.

The "no emerging degree-one CNs" situation may also be found by canceling the nodes and their connected edges from the Tanner graph one by one. More explicitly, this cancelation commences from any of the current degree-one CNs. Using the illustrative lists in Table I as an example, the degree-one CN 3 will be first removed, which is arranged by deleting the contents of its list {3}, making it an empty list. Nonetheless, the list {3} of CN 3 before cancelation implies that the resultant belief may be propagated along the edge to VN 3 during the decoding. Then, based on the list {2, 3} of VN 3, the corresponding belief is conveyed back to CN 2. We refer to this as a completed belief propagation round, commencing from a degree-one CN and flowing back to several other CNs, whose degree will be less

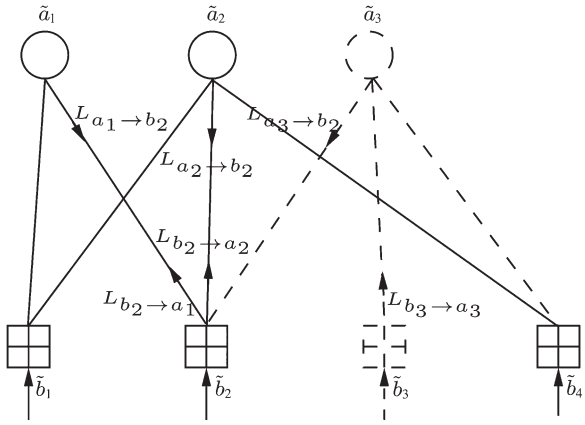

Fig. 3. Enhanced Tanner graph of Fig. 2 generated by adding the extra CN 4, which has a degree of two connecting the just-canceled VN 3 and the VN 2. The VN 2 is connected to CN 1, which has the lowest degree of two among the remainder of the CNs. Here, the parts drawn in the dashed line indicate that they are canceled from the Tanner graph during the process of checking and resolving the structural phenomenon of "no emerging degree-one CNs."

by one. More explicitly, after this completed belief propagation round, the list of VN 3 is also made an empty list, and all edges connected to VN 3 have to be removed from its connected CNs. In this case, its connected CN 2 will remove the index 3 from its list, changing the list from {1, 2, 3} to {1, 2}. In other words, the degree of CN 2 has been decreased from 3 to 2 since the number of indexes in a CN's list indicates that particular CN's degree.

Then, we have to check, whether a new degree-one CN emerges. If a new degree-one CN appears, the same list-nulling actions will be repeated. Otherwise, a new CN needs to be generated, attempting to overcome the current structural phenomenon. Note that the degree of this new CN is not randomly chosen as that of a conventional fountain encoded bit. Instead, it is set to be a degree of two to supply an emerging degree-one CN in succession. In detail, the new CN will have two edges, one of which connects it to the just canceled VN, whereas the other connects it to any one of the VNs, which are connected to the lowest degree CN in the remainder of the Tanner graph. For the example of Fig. 2, the new degree-2 CN is connected to the just-canceled VN 3, as well as to VN 2, which is connected to the current lowest degree CN 1, as shown in Fig. 3. It may be seen that the belief propagation may continue to flow, after producing this new CN 4, which is supposed to have a list of {2, 3}. Yet, its shortened list {2} generated after the removal of the index of 3 will be added to the rest of the Tanner graph for triggering the next cancelations since the VN 3 has been canceled at this moment.

In conclusion, the general process of eliminating the phenomenon of encountering 'no emerging degree-one CNs' ensues as follows.

- Step 1: Attempt to find a degree-one CN. If none exists, go to Step 3.
- Step 2: Cancel the just identified degree-one CN, its connected VN, and all edges of that VN. Then, go to Step 4.
- Step 3: Generate a new degree-two CN, connecting to the just-canceled VN and any one of the VNs connecting to the specific CN, which has the lowest degree in the remainder of the Tanner graph.
- Step 4: Loop to Step 1 until the Tanner graph becomes empty, i.e., it is eliminated.

When the proposed strategies are applied to the fountain codes for solving the structural phenomena of Tanner graphs, the high-degree terms of the degree distribution may be left out for the sake of reducing the average degree since there is no need to worry about uncovered VNs. As discussed in Section II-B3, having high-degree terms in the degree distribution reduces the probability of having uncovered VNs for nonsystematic fountain codes. Therefore, in our simulations discussed in Section III-B, we adopt the following degree distribution for our improved fountain codes:

$$\delta(x) = 0.091717 + 0.493570x + 0.166220x^2 + 0.072646x^3 + 0.082558x^4 + 0.056058x^7 + 0.037229x^8 \quad (6)$$

which was simply formed by adding the weighting coefficients representing the high-degree terms in the degree distribution of Raptor codes in [3] to the weighting coefficient of the degree-one term.

Clearly, we have improved the performance of fountain codes by transmitting a few specifically encoded bits. However, another practical issue has risen: When should the encoder generate these encoded bits during the continuous fountain encoding process? In Section III-B, we chracterized our IRaptor codes based on a fixed coding rate, hence naturally followed by these specifically encoded bits. Furthermore, we proposed a novel IRaptor-coded HARQ scheme detailed in Section IV, where a LUT prestores the most appropriate coding rates for IRaptor codes corresponding to the different channel SNRs of each (re)transmission. Then, these specifically encoded bits can be generated right after the required coding rate has been reached during each (re)transmission.

B. Verifying IRaptor Codes

To characterize the performance of our improved fountain codes, both the PLR achieved and the complexity imposed will be compared with those of conventional fountain codes. We investigated 1) nonsystematic LT codes (LT); 2) systematic Raptor codes (sys Raptor); 3) nonsystematic Raptor codes (Raptor); 4) improved nonsystematic LT codes (ILT); and 5) our improved nonsystematic Raptor codes (IRaptor),[1] by collecting the statistical results after a relevant number of blocks were transmitted, using binary phase-shift keying (BPSK) modulation for transmissions over an additive white Gaussian noise (AWGN) channel. Furthermore, the LTE turbo codes are also used as the most powerful existing benchmarker in our simulations for the sake of comparing its PLR performance

[1]We did not involve systematic LT codes in our simulations since systematic Raptor codes have included an inner systematic LT code and shown higher performance than sole systematic LT codes.

with our IRaptor codes. The short block lengths of 104 and 1008 bits, and the longer length of 4992 bits are considered in our simulations.

The conventional LT codes adopted the classical degree distribution in [3], whereas our improved LT codes relied on (6). For all conventional and IRaptor codes, the coding rate of the outer LDPC codes was set to a high value of 0.9. We employed regular systematic LDPC codes using the parameter set of $(M, 3, 30)$, where M is the number of intermediate bits after the outer LDPC encoding, and 3 is the VN's degree, whereas 30 is the CN's degree in the regular-LDPC Tanner graph. More specifically, the M values for the block lengths of 104 and 1008 bits are 116 and 1120, according to the LDPC coding rate of 0.9. The LDPC codes also employ the sum-product algorithm based on the Tanner graph for decoding [16].

We investigated the performance of these five fountain codes having a fixed coding rate and in conjunction with gradually decreasing coding rates. For the sake of a fair comparison, the overall coding rate of the five fountain codes needs to be kept the same. Hence, the coding rate of the sole LT codes was set to 0.45, whereas the coding rate of the inner LT codes of the Raptor codes was set to 0.5, which is multiplied with the outer 0.9-rate LDPC code rate to have the same overall coding rate of 0.45. Following the conventional fountain encoding process, our improved fountain codes transmit a series of encoded bits until they reach the aforementioned preset coding rate. Then, the encoder reconstructs the Tanner graph using the recorded lists and generates several specifically encoded bits to circumvent the aforementioned structural phenomena, as discussed in Section III-A. Compared with the conventional fountain encoded bits, these extra encoded bits are special since their degree and the VNs involved in the XOR operations are designated, instead of being randomly selected. The receiver uses a pseudorandom generator or side information along with these specifically encoded bits for maintaining synchronization. Nevertheless, our simulation results demonstrated that the influence of these extra encoded bits on the coding rate can be ignored; hence, it remains close to 0.45. Specifically, the coding rate of the improved fountain codes is 0.4498 in our simulations.

The LTE turbo codes adopt two parallel concatenated convolutional codes (CCs) having memory-3 polynomials of $(15, 13)_o$ in octal representation. The two CC encoders output the parity bit sequences $\mathbf{b}_1$ and $\mathbf{b}_2$, respectively, for the systematic bit sequence $\mathbf{a}$ and its interleaved copy. After a series of interleaving operations specified by the LTE standard [15], the interleaved sequence $\mathbf{a}$ followed by the interleaved and combined sequences $\mathbf{b}_1$ and $\mathbf{b}_2$ enter into a circular buffer. The encoded bits are one by one taken from the start position of the circular buffer, until the number satisfies the coding rate of 0.45. The turbo decoder performs the iterative decoding after deinterleaving and depuncturing the received encoded bits, reinstating them into the appropriate bit positions.

For all LT codes and the LTE turbo codes [15], except for the cyclic redundancy check (CRC), the early stopping strategy proposed in [22] was employed for terminating the iterative soft decoding. More specifically, instead of using a fixed number of iterations, the decoder will halt the decoding operations once the incremental contribution of the mutual information (MI) to the extrinsic LLRs of VNs becomes less than 0.0001, as represented by $\mathrm{MI}(L^{(m)}_{a_i \to b_j}) - \mathrm{MI}(L^{(m-1)}_{a_i \to b_j}) < 0.0001$. This is because using more iterations fails to improve the performance but dissipates more battery power. The function $\mathrm{MI}(\cdot)$ is further detailed in [23, Sec. 2.3], which estimates the MI of the extrinsic LLR sequence $L_{a_i \to b_j}$. There are two Tanner graphs in Raptor codes, where one of them is characterizing the inner LT decoding, whereas the other visualizes the outer LDPC decoding operations. More explicitly, following I_{inner} a number of iterations within the inner LT decoding loops, the output *a posteriori* LLRs are subjected to a number of sum-product algorithm iterations performed by the outer LDPC decoder. The given early stopping strategy is also employed for terminating the inner iterative LT decoding, while we invoke $I_{\mathrm{outer}} = 5$ iterations for the outer LDPC decoding, to control the overall complexity. Nevertheless, the iterative LDPC decoding may not have to be invoked at all if the systematic bits representing the original information bits have already satisfied the CRC-based error checking after the inner iterative LT decoding.

Each node in a Tanner graph is related to addition and box-plus calculations. The complexity of fountain codes may be quantified in terms of the total number of addition and box-plus operations per source bit, which are denoted by N_+ and $N_{\boxplus}$, respectively. Note that the total number of operations indicates the number of additions and box-pluses performed during all iterations, not only for the LT codes but for the LDPC codes as well, when considering the complexity of Raptor codes. When relying on the LUT implementation of $f(\cdot)$ in (4), the complexity of box-plus is approximately equal to $[5 + 2 \cdot \log_2(T)]$ additions,[2] where T is the number of entries in the LUT. Referring to [24], when the number of entries becomes $T \geq 4$, the performance of correction-factor-aided min-sum decoding approaches that of the optimum sum-product algorithm, while maintaining low complexity. Therefore, the expression of $(9 \times N_{\boxplus} + N_+)$ may accurately reflect the complexity of fountain codes. This makes it possible for us to compare the complexity of LT codes and Raptor codes.

Given these simulation parameters, Fig. 4(a)–(c) shows the PLR performance for a block length of 104, 1008, and 4992 bits, respectively. Furthermore, Fig. 5(a)–(c) portray the corresponding complexity for three block lengths, where the complexity of all schemes was divided by 1000 for convenient plotting.

For the block length of 104 bits, it may be observed in Fig. 4(a) that our IRaptor codes achieve the lowest PLR among all fountain codes, while having significantly lower complexity compared with the conventional fountain codes. More specifically, the PLR curve of the IRaptor codes decays rapidly, approaching a vanishingly low value upon increasing the SNR. At a PLR of 10^{-3}, our scheme requires 1.5 dB lower SNR than that of the systematic Raptor codes, which have the best performance among the conventional fountain codes. Furthermore, observe in Fig. 4(a) that our improved fountain codes substantially outperform the nonsystematic fountain codes since the

[2]The number of clock cycles performing a single box-plus operation in (4) includes five cycles for comparison operations for obtaining the minimum value between L_1 and L_2 and includes twice searching of the LUT, each of which consumes $\log_2(T)$ cycles.

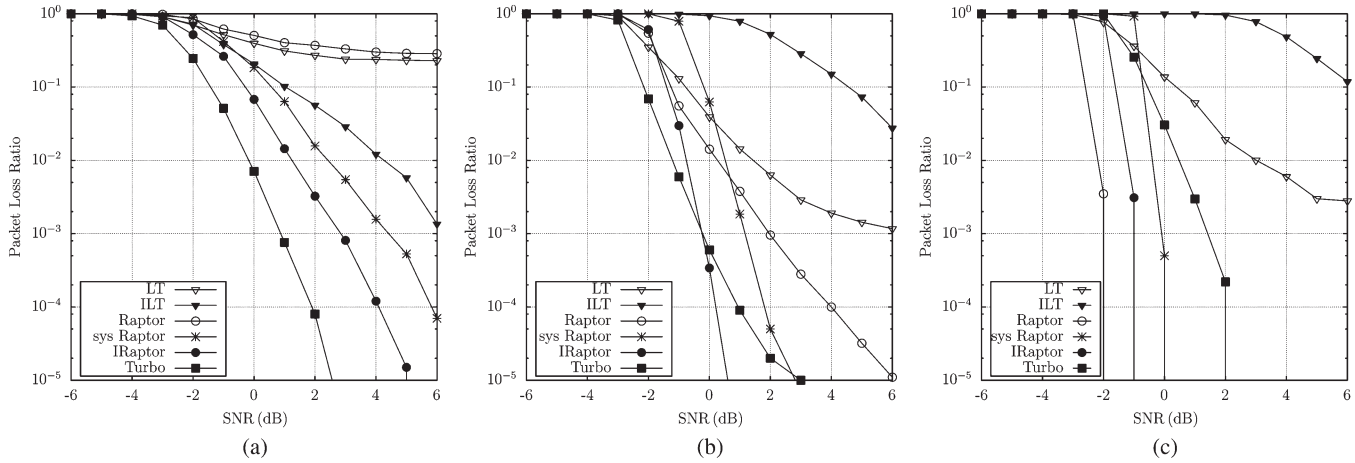

Fig. 4. PLR versus the AWGN channel SNR for the block lengths of (a) 104, (b) 1008, and (c) 4992 bits.

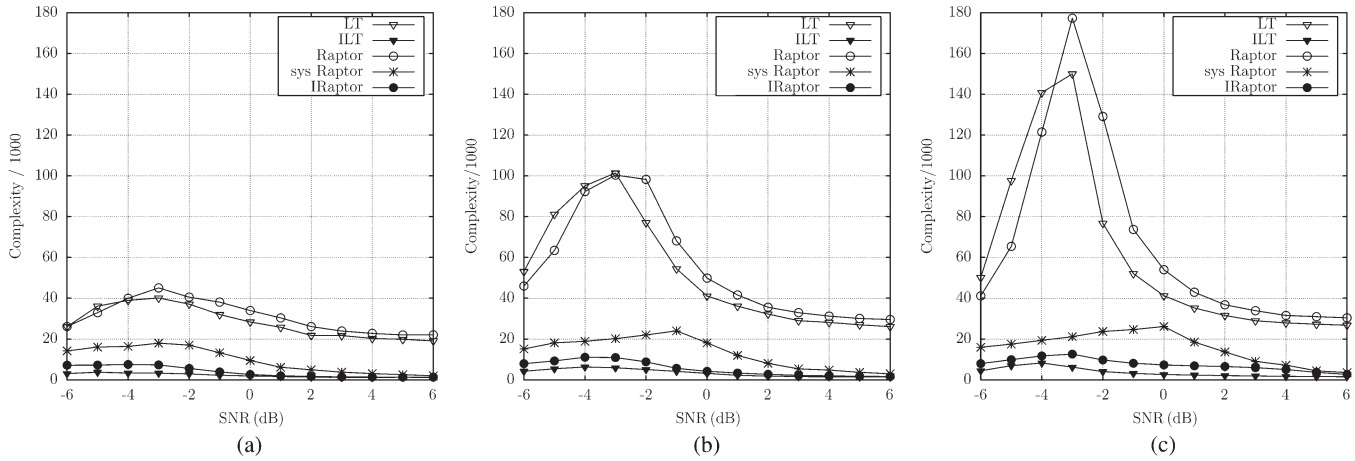

Fig. 5. Complexity versus the AWGN channel SNR for the block lengths of (a) 104, (b) 1008, and (c) 4992 bits.

latter codes have a PLR in excess of 0.2 even at high SNRs. As for the complexity characterized in Fig. 5(a), the improved LT codes impose the lowest complexity among the five fountain codes. The complexity of the IRaptor codes is slightly higher than that of the improved LT codes, owing to the additional LDPC decoding complexity. However, the IRaptor codes still exhibit dramatically reduced complexity, which is less than half of the systematic fountain codes as a benefit of the low-complexity degree distribution of (6).

Although the improved LT code fails to excel for the 1008-bit block length characterized in Fig. 4(b) in terms of its PLR, it imposes the lowest complexity, as shown in Fig. 5(b). This is because the straightforward degree distribution of (6) may not be the optimal one. A low fraction of errors persists in each block after the decoding of the improved LT codes. Nevertheless, these residual errors are likely to be corrected by the outer 0.9-rate LDPC code. Therefore, the IRaptor codes exhibit the best PLR performance among the five fountain codes, as evidenced by Fig. 4(b). The IRaptor codes attain a PLR of 10^{-5} at the SNR of 0 dB, which is 2 dB lower than that required by the conventional systematic Raptor codes and 6 dB lower than the SNR of the nonsystematic Raptor codes. Simultaneously, as shown in Fig. 5(b), the complexity of IRaptor codes is only about half of the conventional systematic Raptor codes. Compared with the conventional nonsystematic fountain codes, the complexity imposed may be reduced by as much as an order of magnitude.

Although our proposed scheme initially aimed for short lengths, our IRaptor codes actually exhibit a desirable performance for the longer 4992-bit codewords. As shown in Fig. 4(c), they have a PLR versus SNR curve that is 1 dB better than that of the systematic Raptor codes, even though it is 1 dB worse than that of the conventional Raptor codes. However, our IRaptor codes achieve the lowest complexity among these three codes, as shown in Fig. 5(c). More explicitly, Fig. 5(c) demonstrates that the complexity of the IRaptor codes may be ten times lower than that of the conventional Raptor codes. Compared with the systematic Raptor codes, the complexity may also be reduced by as much as a factor of 3.5 by our IRaptor codes.

The PLR trend of the LTE turbo codes [15] is also presented in Fig. 4. It can be observed that, in Fig. 4(a), that the LTE turbo code associated with the 104-bit block length outperforms our IRaptor code by about 2 dB. However, for the block length of 1008 bits, it is observed in Fig. 4(b) that the PLR curve of our IRaptor code decays more rapidly than that of the LTE turbo code

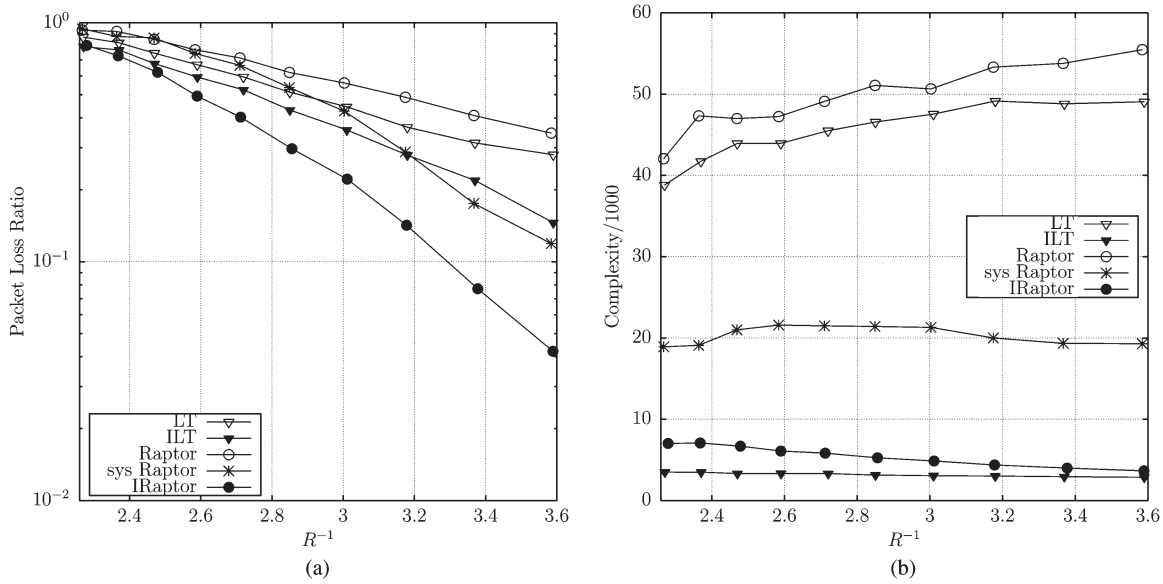

Fig. 6. (a) PLR and (b) complexity versus the reciprocal of the coding rate for the 104-bit block length at the SNR of -3 dB for transmission over AWGN channels.

and exhibits a significantly lower error floor. More specifically, the PLR of our IRaptor codes becomes lower than that of the LTE turbo codes for SNRs in excess of 0 dB, as shown in Fig. 4(b). Furthermore, the PLR versus SNR advantage of our IRaptor codes increases upon increasing the codeword length, which becomes 3 dB better than that of the LTE turbo codes, as shown in Fig. 4(c) for the 4992-bit codewords.

The PLR performance of Fig. 4(b) and (c) confirms that our IRaptor codes may be capable of outperforming the LTE turbo codes when the block length is in excess of 1008 bits, whereas they are outperformed by the LTE scheme in Fig. 4(a) for the short block length of 104 bits. We will further explore the theoretical reason behind this phenomenon in our future work. Note that it is always a challenge to compare two different types of channel codes since a diverse range of contradictory factors should be taken into account, as shown in [25, Fig. 1.3], including the BER/PLR, the complexity, the coding delay, the throughput, etc., and the specific channel characteristics for which the code was designed. In Section IV, a fairer comparison between the LTE turbo codes and our IRaptor codes will be offered in a practical environment, when both of them are combined with an adaptive HARQ scheme, where various coding rates are required for each transmission encountered with different channel conditions in a quasi-static Rayleigh fading channel mode.

Additionally, we explored the candidates' behavior at different coding rates. Fig. 6(a) illustrates the PLR performance versus the reciprocal of the coding rate for the 104-bit block length at the SNR of -3 dB, demonstrating that the IRaptor codes have a significantly lower PLR than the other fountain codes. Specifically, as shown in Fig. 6(a), when the IRaptor codes achieve a PLR of 0.1, the overall coding rate has to be about $1/3.3 = 0.303$. By contrast, the systematic Raptor codes exhibit the best performance among the conventional fountain codes, requiring a coding rate of about $1/3.65 = 0.274$ at the PLR of 0.1. Meanwhile, Fig. 6(b) reveals that the complexity of the IRaptor codes is a factor of three lower than that of the systematic Raptor codes and an order of magnitude lower than that of the nonsystematic fountain codes.

In conclusion, the simulation results here have demonstrated that the IRaptor codes achieve the lowest PLR, despite having lower complexity than that of the conventional fountain codes. This is achieved at the cost of a modestly increased memory requirement during the encoding process at the transmitter. More specifically, this memory is used for storing the lists of all VNs and CNs, whereas a few additional operations are involved in going through these lists for generating several specifically encoded bits, as discussed in Section III-A.

IV. Adaptive IRaptor-Coded Hybrid Automatic Repeat Request

Traditional HARQ has a fixed coding rate for each of its (re)transmissions, each of which may encounter different channel conditions when a quasi-static Rayleigh fading channel model is considered. Therefore, a fixed-rate HARQ scheme may not be capable of making an efficient use of the specific channel conditions that occur within all (re)transmissions. Moreover, the retry limit of the fixed-rate HARQ constrains the overall coding rate, which may result in unsuccessful decoding, when the channel conditions of all (re)transmissions are hostile. In this case, the packet will be deemed lost despite all the (re)transmissions. Hence, both the PLR and the throughput suffer.

The straightforward solution is to use an adaptive HARQ scheme, which may invoke different coding rates for each (re)transmission, bearing in mind the specific channel conditions encountered. This requires that the transmitter should know the channel quality before its transmission and that the channel code is capable of supporting arbitrary coding rates. In the LTE system [15], CQI messages are used for indicating the channel states for appropriately configuring its adaptive

TABLE II
CODING RATES OF IRAPTOR CODES, AIMING FOR A PLR OF 0.1 WHEN THE PACKET LENGTH IS 104-bit

SNR(dB)	-12.0	-11.0	-10.0	-9.0	-8.0	-7.0	-6.0	-5.0	-4.0
R	0.05	0.07	0.08	0.10	0.13	0.16	0.2	0.24	0.29

SNR(dB)	-3.0	-2.0	-1.0	0.0	1.0	2.0	3.0	4.0	5.0	6.0
R	0.34	0.41	0.47	0.54	0.61	0.68	0.75	0.82	0.89	1

modulation scheme before transmission. They may be beneficially utilized by our IRaptor-coded HARQ scheme proposed here by exploiting its rateless property. The minimum required number of encoded symbols was theoretically studied for a Raptor-coded HARQ scheme in [26]. By contrast, in our IRaptor HARQ, a LUT will be designed in the following for prestoring all the required coding rates.

A. LUT Design

Again, we carefully design a LUT for the IRaptor-coded HARQ scheme, which prestores the coding rates of IRaptor codes required for different SNRs. Using these coding rates, a PLR of about 0.1 may be achieved for transmissions over an AWGN channel. This LUT may be generated by an offline training process, which relies on transmitting a sufficiently high number of IRaptor encoded packets at various coding rates, as described in Section III-B. Table II shows an example of the LUT designed for the SNR range spanning from -12 to 6 dB for the packet length of 104 bits.

According to the LUT shown in Table II, a low coding rate is required for guaranteeing a high probability of successful reception, if a specific transmission attempt occurs in a deep fade. For example, a coding rate as low as 0.05 is required for the SNR of -12 dB. This may however significantly degrade the effective throughput. If a HARQ scheme avoids transmissions in deep fades, and instead it opts for transmitting during better channel conditions within the allowed retransmission limit, it will achieve both a high effective throughput and a desirable PLR performance.

B. HARQ Flow

Based on the given analysis, our proposed IRaptor-coded HARQ deactivates potentially futile transmissions when the channel experiences a deep fade, or continues transmitting, until the number of IRaptor encoded bits becomes capable of guaranteeing a low PLR. The channel condition may be identified by a short CQI message, which characterizes the SNR estimated by the receiver.

A short CQI message carrying the estimated SNR will be fed back from the receiver to the transmitter before its next transmission. If the estimated SNR is higher than a threshold SNR $\sigma_{\rm th}$, the transmitter will search through the LUT in order to find the most appropriate coding rate. Then, it continues transmitting the IRaptor encoded bits, until that specific coding rate has been reached. After that, it will reconstruct the Tanner graph and transmits several specifically encoded bits for overcoming its potential structural phenomena, as described in Section III-A. Otherwise, if the estimated SNR is lower than $\sigma_{\rm th}$, the transmitter waits to time out by disabling this transmission. The next retransmission may then be triggered in this situation. The retransmission may also be triggered without receiving an acknowledgement (ACK) message from the receiver until the retry limit is reached.

The receiver is responsible for detecting the channel quality and for sending the CQI message back. It will then execute iterative decoding based on all the received encoded bits. If the CRC is satisfied, the receiver sends an ACK message back to the transmitter; otherwise, it waits for the next retransmission or discards the packet if the maximum retransmission limit is exhausted.

The threshold SNR $\sigma_{\rm th}$ is used for indicating a deep fade. Its value strikes a tradeoff between the attainable throughput and the PLR encountered, where the throughput is defined as a ratio of the number of successfully received information bits over the total number of transmitted bits from the upper layer's perspective. If the threshold SNR $\sigma_{\rm th}$ is set to a low value, the packets may be delivered even in a deep fade, but this results in a low coding rate. Hence, it guarantees a low PLR, but as a price, the attainable throughput suffers. By contrast, for a high $\sigma_{\rm th}$ value, transmission opportunities may be missed even for transmission over a relatively benevolent channel when the estimated SNR is below $\sigma_{\rm th}$. For example, let us consider the threshold SNRs of $\sigma_{\rm th} = -12$ dB and $\sigma_{\rm th} = -8$ dB, as well as the estimated SNR of -10 dB. Then, transmissions are avoided for $\sigma_{\rm th} = -8$ dB, since we have $-10 < -8$. By contrast, for $\sigma_{\rm th} = -12$ dB, we have $-10 > -12$, hence, the packet's transmission may become successful when using the low coding rate of 0.08 corresponding to -10 dB, as shown in Table II.

C. Simulation Results

We developed simulations for investigating both the throughput and PLR trends of our proposed IRaptor-coded HARQ scheme for the threshold SNR values in the set of $\{-12, -10,$ and -8 dB$\}$, which were shown in Figs. 7 and 8. Furthermore, we applied our new adaption mechanism to the LTE turbo-coded HARQ as a benchmarker for comparison. To exploit the advantages of adaptive HARQ schemes, the fixed-rate LTE turbo HARQ and our fixed-rate IRaptor HARQ are also characterized in Figs. 7 and 8.

For all HARQ schemes, the ARQ-retry limit was set to 4. A sufficiently high number of packets having an original information length of 104 bits were BPSK modulated and transmitted over a quasi-static, i.e., block-fading Rayleigh channel. In the implementation of adaptive HARQ schemes, the real value of each estimated SNR was rounded down to the closest integer for determining the coding rate using our LUT. For example, an estimated SNR of 0.65 dB was rounded down to the SNR of 0 dB.

The LTE HARQ scheme is based on the turbo codes described in Section III-B. In our simulations, the fixed-rate LTE

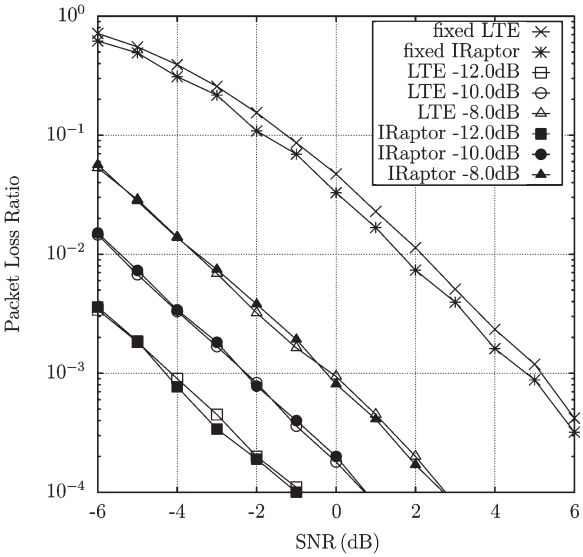

Fig. 7. PLR versus SNR for all candidate HARQ schemes for transmission over a quasi-static Rayleigh fading channel.

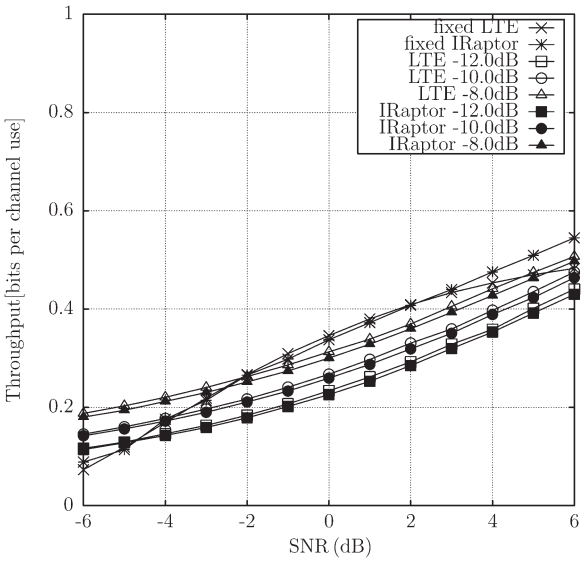

Fig. 8. Throughput versus SNR for all candidate HARQ schemes for transmission over a quasi-static Rayleigh fading channel.

HARQ employs the coding rate of 1 for each (re)transmission. More specifically, the transmitter transmits 104 bits for each of its four (re)transmissions, which are sequentially provided by the circular buffer by advancing its starting position. At the receiver, Chase combining is carried out for the repeated LLRs received from all (re)transmissions. When our adaptive mechanism is applied to the LTE HARQ, the coding rates in the LUT of Table II are reused for different channel qualities for the sake of fair comparison. The number of transmitted bits corresponding to the coding rate may be obtained by circularly forwarding the starting position along the circular buffer. This circular operation aids the turbo-coded HARQ easily satisfy any arbitrary coding rates. Therefore, Chase combining is potentially required for the repetitions in a single transmission if this transmission requires the coding rate less than 1/3, which implies the starting position has been advanced along the circular buffer more than one circle. In both the fixed-rate and the adaptive LTE HARQ, iterative decoding will be executed between two Bahl, Cocke, Jelinek, and Raviv (BCJR) decoders until the CRC is satisfied or the MI is converged.

Observe from Fig. 8 that, although the fixed-rate IRaptor-coded HARQ has a similar throughput to that of the LTE system's fixed-rate turbo coded HARQ scheme, its PLR is slightly lower, as shown in Fig. 7. Alternatively, we can say that it requires an approximately 0.5 dB lower SNR for maintaining the same PLR. However, Fig. 7 demonstrated that a significantly lower PLR may be achieved by the adaptive HARQ arrangement right across the entire SNR range, regardless of whether our adaptive IRaptor HARQ or the LTE adaptive HARQ is used, explicitly around 5-dB lower power may be used than those of the nonadaptive HARQ, even for the highest threshold of $\sigma_{\rm th} = -8$ dB. More specifically, when the threshold SNR $\sigma_{\rm th}$ is set for example to -12 dB, the PLR is below 10^{-3} for SNRs in excess of -4 dB. The PLR performance curve is shifted to the right by about 2 dB for the threshold SNR $\sigma_{\rm th}$ of -10 dB, whereas the throughput observed in Fig. 8 exhibits an improvement of about 4%.

Note that the LTE adaptive HARQ scheme can be seen to offer a similar PLR as our IRaptor HARQ scheme in Fig. 7. Furthermore, Fig. 8 shows that both schemes facilitate similar *transmission* throughputs. However, our IRaptor scheme has a significant advantage over the LTE adaptive HARQ scheme in terms of *processing* throughput and latency. More specifically, turbo decoders rely on the BCJR algorithm, which employs recursive calculations up and down the length of the trellis [27]. These forward and backward recursions lead to lots of data dependence, which prevent very parallel processing in the turbo decoder hardware. In state-of-the-art turbo decoder implementations [28], only 64 trellis stages can be processed in each hardware clock cycle, resulting in an iterative turbo decoding process that takes hundreds or thousands of clock cycles to complete, depending on the frame length. By contrast, the decoder of our IRaptor scheme is based upon a factor graph, in which there are significantly fewer data dependencies. This allows all of the VNs to be processed simultaneously in parallel, and then all of the CNs to be processed simultaneously, in parallel [29], [30]. Owing to this, the iterative decoding process can be completed in only tens of clock cycles if a sufficiently parallel processing architecture is employed (at the cost of having a large chip area). Indeed, in [28], [31], and [32], it is shown that LDPC decoders based on factor graphs can be implemented with processing throughputs of tens of gigabits per second, whereas the fastest BCJR-based turbo decoders have throughputs of only 1 or 2 Gbit/s. In summary, our IRaptor scheme can be expected to facilitate an order-of-magnitude improvement to the processing throughput and latency of the LTE adaptive HARQ scheme, while maintaining the same PLR and transmission throughput.

V. Conclusion

The family of rateless Fountain codes has been conceived for filling packet erasures for transmission over BECs. However,

owing to their suboptimum Tanner graph structure, their performance erodes when they act as channel codes in the physical layer of noise-contaminated fading channels. To circumvent this impediment, we conceived a beneficial technique for incorporating several specifically encoded bits, which are generated for eliminating the structural imperfections of their Tanner graph. The resultant IRaptor codes exhibit an excellent PLR performance, despite their low complexity.

Furthermore, a powerful IRaptor-coded LUT-aided HARQ scheme was proposed for block-fading channels, where the most appropriate code rate to be used was determined using a LUT based on the estimated SNR. When considering our rateless-coded HARQ scheme, the potentially infinite number of coding rates is reduced to a finite number stored in our LUT. In our future work, we may embark on tackling the challenge of finding the most appropriate Tanner graph connection pattern corresponding to each specific coding rate for various packet lengths.

REFERENCES

[1] D. J. C. MacKay, "Fountain codes," *Proc. Inst. Elect. Eng.—Commun.*, vol. 152, no. 6, pp. 1062–1068, Dec. 2005.

[2] M. Luby, "LT codes," in *Proc. 43rd Annu. IEEE Symp. Found. Comput. Sci.*, 2002, pp. 271–280.

[3] A. Shokrollahi, "Raptor codes," *IEEE Trans. Inf. Theory*, vol. 52, no. 5, pp. 2033–2051, May 2006.

[4] U. Erez, M. Trott, and G. Wornell, "Rateless coding for Gaussian channels," *IEEE Trans. Inf. Theory*, vol. 58, no. 2, pp. 530–547, Feb. 2012.

[5] T.-Y. Chen, D. Divsalar, J. Wang, and R. Wesel, "Protograph-based raptor-like LDPC codes for rate compatibility with short blocklengths," in *Proc. IEEE GLOBECOM Conf.*, 2011, pp. 1–6.

[6] R. Palanki and J. Yedidia, "Rateless codes on noisy channels," in *Proc. ISIT*, Jun. 2004.

[7] J. Castura and Y. Mao, "Rateless coding over fading channels," *IEEE Commun. Lett.*, vol. 10, no. 1, pp. 46–48, Jan. 2006.

[8] O. Etesami and A. Shokrollahi, "Raptor codes on binary memoryless symmetric channels," *IEEE Trans. Inf. Theory*, vol. 52, no. 5, pp. 2033–2051, May 2006.

[9] K. Hu, J. Castura, and Y. Mao, "Performance-complexity tradeoffs of Raptor codes over Gaussian channels," *IEEE Commun. Lett.*, vol. 11, no. 4, pp. 343–345, Apr. 2007.

[10] B. Sivasubramanian and H. Leib, "Fixed-rate Raptor codes over Rician fading channels," *IEEE Trans. Veh. Technol.*, vol. 57, no. 6, pp. 3905–3911, Nov. 2008.

[11] Z. Cheng, J. Castura, and Y. Mao, "On the design of Raptor codes for binary-input Gaussian channels," *IEEE Trans. Commun.*, vol. 57, no. 11, pp. 3269–3277, Nov. 2009.

[12] K. Kasai and K. Sakaniwa, "Fountain codes with multiplicatively repeated non-binary LDPC codes," in *Proc. 6th ISTC Iterative Inf. Process.*, 2010, pp. 374–378.

[13] R. Tanner, "A recursive approach to low complexity codes," *IEEE Trans. Inf. Theory*, vol. 27, no. 5, pp. 533–547, Sep. 1981.

[14] X. Yuan and L. Ping, "On systematic LT codes," *IEEE Commun. Lett.*, vol. 12, no. 9, pp. 681–683, Sep. 2008.

[15] "3rd Generation Partnership Project; Technical Specification group radio access network; Evolved Universal Terrestrial Radio Access (E-UTRA); Multiplexing and channel coding (Release 10)," 3GPP TS 36.212, Sophia Antipolis Cedex, France, Dec. 2010. [Online]. Available: http://www.3gpp.org/FTP/Specs/html-info/26346.htm

[16] F. Kschischang, B. Frey, and H.-A. Loeliger, "Factor graphs and the sum-product algorithm," *IEEE Trans. Inf. Theory*, vol. 47, no. 2, pp. 498–519, Feb. 2001.

[17] H. Jenkač and T. Mayer, "Soft decoding of LT-codes for wireless broadcast," in *Proc. IST Mobile Summit*, Jun. 2005.

[18] X. Liu and T. J. Lim, "Fountain codes over fading relay channels," *IEEE Trans. Wireless Commun.*, vol. 8, no. 6, pp. 3278–3287, Jun. 2009.

[19] N. Bonello, R. Zhang, S. Chen, and L. Hanzo, "Reconfigurable rateless codes," *IEEE Trans. Wireless Commun.*, vol. 8, no. 11, pp. 5592–5600, Nov. 2009.

[20] J. Hagenauer, E. Offer, and L. Papke, "Iterative decoding of binary block and convolutional codes," *IEEE Trans. Inf. Theory*, vol. 42, no. 2, pp. 429–445, Mar. 1996.

[21] S. Tong, P. Wang, D. Wang, and X. Wang, "Box-minus operation and application in sum-product algorithm," *Electron. Lett.*, vol. 41, no. 4, pp. 197–198, Feb. 2005.

[22] H. Chen, R. G. Maunder, and L. Hanzo, "Low-complexity multiple-component turbo decoding aided hybrid ARQ," *IEEE Trans. Veh. Technol.*, vol. 60, no. 4, pp. 1571–1577, May 2011.

[23] J. Hagenauer, "The EXIT chart—Introduction to extrinsic information transfer in iterative processing," in *Proc. 12th EUSIPCO*, 2004, pp. 1541–1548.

[24] X. Zuo, R. Maunder, and L. Hanzo, "Design of fixed-point processing based LDPC codes using EXIT charts," in *Proc. IEEE VTC—Fall*, Sep. 2011, pp. 1–5.

[25] L. Hanzo, T. Liew, B. Yeap, R. Tee, and S. Ng, *Turbo Coding, Turbo Equalisation and Space-Time Coding: EXIT-Chart-Aided Near-Capacity Designs for Wireless Channels*, 3rd ed. Hoboken, NJ, USA: Wiley, 2011.

[26] E. Soijanin, N. Varnica, and P. Whiting, "Punctured vs rateless codes for hybrid ARQ," in *Proc. IEEE ITW Punta del Este.*, Mar. 2006, pp. 155–159.

[27] L. Hanzo, J. P. Woodard, and P. Robertson, "Turbo decoding and detection for wireless applications," *Proc. IEEE*, vol. 95, no. 6, pp. 1178–1200, Jun. 2007.

[28] T. Ilnseher, F. Kienle, C. Weis, and N. Wehn, "A 2.15 Gbit/s turbo code decoder for LTE advanced base station applications," in *Proc. Int. Symp. Turbo Codes Iterative Inf. Process.*, Gothenburg, Sweden, Aug. 2012, vol. 1, pp. 21–25.

[29] C. Howland and A. Blanksby, "Parallel decoding architectures for low density parity check codes," in *Proc. IEEE ISCAS*, May 2001, vol. 4, pp. 742–745.

[30] F. Verdier and D. Declercq, "A low-cost parallel scalable FPGA architecture for regular and irregular LDPC decoding," *IEEE Trans. Commun.*, vol. 54, no. 7, pp. 1215–1223, Jul. 2006.

[31] N. Onizawa, T. Hanyu, and V. Gaudet, "Design of high-throughput fully parallel LDPC decoders based on wire partitioning," *IEEE Trans. VLSI Syst.*, vol. 18, no. 3, pp. 482–489, Mar. 2010.

[32] V. Chandrasetty and S. Aziz, "FPGA implementation of a LDPC decoder using a reduced complexity message passing algorithm," *J. Netw.*, vol. 6, no. 1, pp. 36–45, Jan. 2011.

Hong Chen received the Master's degree in computer science from the University of Electronic Science and Technology (UESTC), Chengdu, China, and the Ph.D. degree from the Communications Research Group, School of Electronics and Computer Science, University of Southampton, Southampton, U.K.

Since 2000, she has been a Lecturer with UESTC. Upon the completion of her doctoral studies, she became a Postdoctoral Research Fellow with the University of Surrey, Guildford, U.K. Her current research interests include cross-layer optimization of wireless networks and turbo-coding-aided hybrid automatic repeat request.

Robert G. Maunder (M'03) received the B.Eng. degree in electronic engineering and the Ph.D. degree in wireless communications from the University of Southampton, Southampton, U.K., in 2003 and 2007, respectively.

He is currently with the School of Electronics and Computer Science, University of Southampton, Southampton, U.K. He is the author of a number of IEEE papers in these areas. His research interests include video coding, joint source/channel coding, and iterative decoding.

Yi Ma (M'04–SM'10) received the Ph.D. degree in electrical engineering and electronics from The University of Liverpool, Liverpool, U.K., in 2004.

Since 2004, he has been with the Institute for Communication Systems (ICS), University of Surrey, Guildford, U.K., where he is currently a member of the academic staff. He is leading a research group within the ICS to conduct the basic-level communication systems research, covering signal processing and applied information theory for wireless communications. He is the Chair of the Air Interface Club within the ICS. He is the author or coauthor of more than 100 peer-reviewed IEEE journal and conference papers in the areas of cooperative communications, cognitive radios, interference utilization, cooperative localization, radio resource allocation, multiple-input multiple-output, estimation, synchronization, modulation, and detection techniques. He has three patents in the areas of spectrum sensing, signal modulation, and detection. He is currently the Technical Coordinator of FP7 ICT-RESCUE project.

AQ4

Rahim Tafazolli (SM'09)

He is currently the Director of the Institute for Communication Systems and of the 5G Innovation Centre, University of Surrey, Guildford, U.K. He is the author of more than 500 research papers in refereed journals and international conferences and has served as an invited speaker. He currently has more than 20 patents in the field of mobile communications. He is the editor of two books on *Technologies for Wireless Future*. He has also worked as a consultant to many mobile companies. He brings his international standing in the communications technology academic and industrial community and his expert technical knowledge of the field to the project.

Mr. Tafazolli is a Fellow of The Institution of Engineering and Technology and Wireless World Research Forum. He has lectured, chaired, and been invited as a keynote speaker to a number of IET and IEEE workshops and conferences. He currently serves as the Chair for the EU Net!Works Technology Platform Expert Group, as a board member of the U.K. Future Internet Strategy Group, and as a Coordinator of the IoT-i Coordination Action Project.

Lajos Hanzo (F'04) received the Master's degree in electronics, the Ph.D. degree, and the *Doctor Honoris Causa* degree from the Technical University of Budapest, Budapest, Hungary, in 1976, 1983, and 2009 respectively, and the D.Sc. degree from the University of Southampton, Southampton, U.K., in 2004.

During his career in telecommunications, he has held various research and academic posts in Hungary, Germany, and the U.K. Since 1986, he has been with the School of Electronics and Computer Science, University of Southampton, Southampton, U.K., where he holds the Chair in telecommunications. He was a Chaired Professor of Tsinghua University, Beijing, China. He is the coauthor of 20 John Wiley/IEEE Press books on mobile radio communications, totalling in excess of 10 000 pages, and has published more than 1400 research entries on IEEE Xplore. He is currently directing an academic research team, working on a range of research projects in the field of wireless multimedia communications sponsored by industry, the Engineering and Physical Sciences Research Council (EPSRC) U.K., the European IST Program, and the Mobile Virtual Centre of Excellence, U.K. He is an enthusiastic supporter of industrial and academic liaison, and he offers a wide range of industrial courses.

Dr. Hanzo has acted as a Technical Program Committee Chair for IEEE conferences, presented keynote lectures, and has received a number of distinctions. He is the Governor of the IEEE Vehicular Technology Society and the Past Editor-in-Chief of the IEEE Press.

AUTHOR QUERIES

AUTHOR PLEASE ANSWER ALL QUERIES

AQ1 = Please provide keywords
AQ2 = Please provide page range and location for Ref. [6].
AQ3 = Please provide page range and location for Ref. [17].
AQ4 = Kindly provide the academic history of R. Tafazolli.

END OF ALL QUERIES